Journal of Magnetics 23(1), 35-40 (2018)

ISSN (Print) 1226-1750
ISSN (Online) 2233-6656
https://doi.org/10.4283/JMAG.2018.23.1.035

Interaction Forces and Torques between Two Perpendicular Magnetic Tubes

Jian-Gang Li*

College of Engineering, Yanbian University, Yanji 133002, China

(Received 19 September 2017, Received in final form 8 February 2018, Accepted 13 February 2018)

Cylinders, tubes, cuboids, etc. are basic magnet shapes used in permanent magnet machines. The relative positions between magnets include parallel, perpendicular, or inclined. The force and torque between two cuboid magnets of almost any status and two cylindrical magnets with paralleled axes have been solved. Using the theory of magnetic charges and magnetic Coulomb's law, this study derives a mathematical model for interaction forces and torques between two perpendicular magnetic tubes in three dimensions. Using this model, the effects of tube relative positions on the interaction forces and torques is analyzed by numerical calculation. The model can also express interaction forces and torques between a magnetic tube and magnetic cylinder or between two magnetic cylinders when the inner radius of one magnetic tube is zero or the radii of both tubes are zero. This study provides the theoretical background for magnetic tube and cylinder applications, such as magnetic drive or control across space in mechanical, medical treatment, chemical industry, food production, aerospace, etc.

Keywords : magnetic charges, Coulomb's law, magnetic tube, magnetic force, magnetic torque

1. Introduction

In some applications, such as magnetic bearings, pumps, couplings, springs, medical instruments, etc. [1-6], the calculation of interaction force, torque and field is very important [7-13]. The interaction is related to shape, magnetization direction, magnetic polarization, and relative position of the permanent magnets outside the magnet dimensions.

For parallel or perpendicular cuboidal permanent magnets, analytical models of the interaction forces and torques were established from the interaction energy between the magnets [14-17], and experimentally verified. Analytical expressions for the torque on cuboidal permanent magnets were obtained using the Lorentz force method [18], and torque of a permanent magnet coupling was derived using the analytical formula of the tangential force [19]. The gyroscopic moment of a passive magnetic axial bearing with Halbach magnetized array (constituting of some cuboidal magnets) was calculated using a two-dimensional finite element method [10].

For cylindrical permanent magnets, the magnetic force between two coaxial/parallel magnets has been calculated assuming uniform magnetization and studied by magnetostatic interaction energy [20], Kelvin's formula [21], Ampere's formula [22], and Lorentzian model [23], respectively. The analytical expression of the attractive force between two arrays of cylindrical permanent magnets was derived from the derivative of the total magnetostatic interaction energy with respect to the axial coordinate [24, 25]. Interaction energy and force between two parallel thin magnetic nanotubes with axial magnetization have been calculated by four different approaches [26]. The interaction energy, and axial and radial interaction forces have been expressed semi-analytically in magnetostatic interaction energy when a cylindrical permanent magnet is inside a tubular permanent magnet [27]. For two tube shaped magnets, the interaction force between two coaxial magnets with the same magnetization, used as magnetic bearings, has been investigated using the theory of magnetic charges and magnetic Coulomb's law [28, 29], as has the attractive force between two coaxial cylindrical magnets with opposite axial magnetizations [30]. Transmitting torque and synchronization of plane type magnet couplings, consisting of a number of couples of magnetic poles, have been studied theoretically and experimentally [31].

However, interaction force and torque between two perpendicular magnetic tubes or cylinders is rarely reported. This paper derives the models of force and torque

*Corresponding author: Tel: +86-13039337073
Fax: +86-433-2732258, e-mail: jgli@ybu.edu.cn

between two perpendicular magnetic tubes using the theory of magnetic charges and magnetic Coulomb's law, and the method for numerical calculation of the magnetic force using the theory of magnetic charges has been experimental verified many times [28-31].

2. Mathematical model

2.1. Forces between two perpendicular magnetic tubes

Figure 1 shows the geometry considered for the perpendicular magnetic tubes. The tubes are made of NdFeB permanent magnets, with tube axes perpendicular to each other in three dimensions. Magnetizations $\vec{J}_1$ and $\vec{J}_2$ are along the tube axes and assumed to be rigid and uniform in each magnetic tube. O and O_2 are the centers of the first ($\mathrm{MT_I}$) and second ($\mathrm{MT_{II}}$) magnetic tube, and they are also the origins of the coordinates $Oxyz$ and O_2y_2. For $\mathrm{MT_I}$, length, and inner and outer radii = $2l_1$, R_{1i} and R_{1o}, respectively. For $\mathrm{MT_{II}}$, length, and inner and outer radii = $2l_2$, R_{2i}, and R_{2o}, respectively. The center of $\mathrm{MT_{II}}$ (O_2) is relative to the center of $\mathrm{MT_I}$ (O) along the three axes of $Oxyz$, expressed by x_0, y_0 and z_0, respectively, and axis O_2y_2 is inclined to axis Oy, expressed by angle γ.

S_1 and S_3 are the South Poles of $\mathrm{MT_I}$ and $\mathrm{MT_{II}}$, as well as S_2 and S_4 are the North Poles of $\mathrm{MT_I}$ and $\mathrm{MT_{II}}$, respectively. Magnetization directions $\vec{J}_1$ and $\vec{J}_2$ are perpendicular in three dimensions, as shown in Fig. 1. The magnetic charge density on the side surfaces of the two tubes is $\sigma = +J$ (North Pole) and $-\sigma = -J$ (South Pole). For rare-earth permanent magnets, magnetic charge

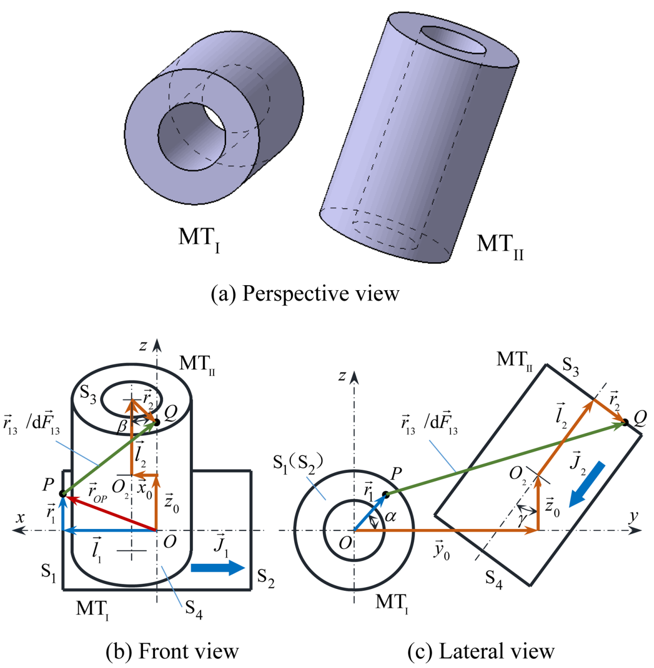

Fig. 1. (Color online) Magnetic tubes configuration.

face density can be expressed as $\sigma = B_r$, where B_r is the remanence of permanent magnets. P is a micro-unit area on the South Pole surface of $\mathrm{MT_I}$. Area = $r_1\mathrm{d}r_1\mathrm{d}\alpha$, and its magnetic charges can be expressed by $-B_{r1}r_1\mathrm{d}r_1\mathrm{d}\alpha$. Similarly, magnetic charges at point Q on the South Pole of $\mathrm{MT_{II}}$ can be expressed by $-B_{r2}r_2\mathrm{d}r_2\mathrm{d}\beta$. Where $\vec{r}_1$ is the vector from the center of S_1 to point P, $\vec{r}_2$ is the vector from the center of S_3 to point Q, α and β are the azimuthal angle of vector $\vec{r}_1$ and $\vec{r}_2$, respectively. Thus, from the magnetic Coulomb's law, interaction forces between two micro-unit areas in the four sided surface can be expressed as

$$\begin{cases} \mathrm{d}\vec{F}_{13} = \dfrac{(-B_{r1})\times(-B_{r2})}{4\pi\mu_0}\cdot\dfrac{r_1r_2\mathrm{d}r_1\mathrm{d}r_2\mathrm{d}\alpha\mathrm{d}\beta}{\left|\vec{r}_{13}\right|^3}\cdot\vec{r}_{13} \\ \mathrm{d}\vec{F}_{14} = \dfrac{(-B_{r1})\times(+B_{r2})}{4\pi\mu_0}\cdot\dfrac{r_1r_2\mathrm{d}r_1\mathrm{d}r_2\mathrm{d}\alpha\mathrm{d}\beta}{\left|\vec{r}_{14}\right|^3}\cdot\vec{r}_{14} \\ \mathrm{d}\vec{F}_{23} = \dfrac{(+B_{r1})\times(-B_{r2})}{4\pi\mu_0}\cdot\dfrac{r_1r_2\mathrm{d}r_1\mathrm{d}r_2\mathrm{d}\alpha\mathrm{d}\beta}{\left|\vec{r}_{23}\right|^3}\cdot\vec{r}_{23} \\ \mathrm{d}\vec{F}_{24} = \dfrac{(+B_{r1})\times(+B_{r2})}{4\pi\mu_0}\cdot\dfrac{r_1r_2\mathrm{d}r_1\mathrm{d}r_2\mathrm{d}\alpha\mathrm{d}\beta}{\left|\vec{r}_{24}\right|^3}\cdot\vec{r}_{24} \end{cases}, \tag{1}$$

where μ_0 is permeability of vacuum, $\mu_0 = 4\pi\times10^{-7}$ $(\mathrm{H\cdot m^{-1}})$; $\mathrm{d}\vec{F}_{13}$ is the differential magnetic force between two micro-unit areas, P (on the face of S_1) and Q (on the face of S_3), $\vec{r}_{13}$ is the vector of P to Q, $\left|\vec{r}_{13}\right|$ is the mode of vector $\vec{r}_{13}$. Similarly, there are differential magnetic forces $\mathrm{d}\vec{F}_{14}$, $\mathrm{d}\vec{F}_{23}$, and $\mathrm{d}\vec{F}_{24}$, the vectors $\vec{r}_{14}$, $\vec{r}_{23}$, and $\vec{r}_{24}$, and the modes $\left|\vec{r}_{14}\right|$, $\left|\vec{r}_{23}\right|$, and $\left|\vec{r}_{24}\right|$.

The projection form of $\mathrm{d}\vec{F}_{13}$ is

$$\begin{cases} \mathrm{d}F_{13x} = \dfrac{(-B_{r1})\times(-B_{r2})}{4\pi\mu_0}\cdot\dfrac{r_1r_2\mathrm{d}r_1\mathrm{d}r_2\mathrm{d}\alpha\mathrm{d}\beta}{\left|\vec{r}_{13}\right|^3}\cdot r_{13x} \\ \mathrm{d}F_{13y} = \dfrac{(-B_{r1})\times(-B_{r2})}{4\pi\mu_0}\cdot\dfrac{r_1r_2\mathrm{d}r_1\mathrm{d}r_2\mathrm{d}\alpha\mathrm{d}\beta}{\left|\vec{r}_{13}\right|^3}\cdot r_{13y} \\ \mathrm{d}F_{13z} = \dfrac{(-B_{r1})\times(-B_{r2})}{4\pi\mu_0}\cdot\dfrac{r_1r_2\mathrm{d}r_1\mathrm{d}r_2\mathrm{d}\alpha\mathrm{d}\beta}{\left|\vec{r}_{13}\right|^3}\cdot r_{13z} \end{cases}, \tag{2}$$

where r_{13x}, r_{13y}, and r_{13z} are the projections of $\vec{r}_{13}$ to the Ox, Oy, and Oz axes, respectively; and the projection forms of $\mathrm{d}\vec{F}_{14}$, $\mathrm{d}\vec{F}_{23}$, and $\mathrm{d}\vec{F}_{24}$ can be similarly expressed, but are not shown here for space considerations.

The differential form of the interaction force along the three axes is

$$\begin{cases} \mathrm{d}F_x = \mathrm{d}F_{13x} + \mathrm{d}F_{14x} + \mathrm{d}F_{23x} + \mathrm{d}F_{24x} \\ \mathrm{d}F_y = \mathrm{d}F_{13y} + \mathrm{d}F_{14y} + \mathrm{d}F_{23y} + \mathrm{d}F_{24y} \\ \mathrm{d}F_z = \mathrm{d}F_{13z} + \mathrm{d}F_{14z} + \mathrm{d}F_{23z} + \mathrm{d}F_{24z} \end{cases}. \tag{3}$$

Combining Eqs. (1) and (2), then substituting the result into Eq. (3), the integral form of the forces can be expressed as

$$\begin{cases} F_x = \dfrac{B_{r1}B_{r2}}{4\pi\mu_0} \cdot \int_{R_{1i}}^{R_{1o}}\int_{R_{2i}}^{R_{2o}}\int_0^{2\pi}\int_0^{2\pi} \left(+ \dfrac{r_{13x}}{|\vec{r}_{13}|^3} - \dfrac{r_{14x}}{|\vec{r}_{14}|^3} - \dfrac{r_{23x}}{|\vec{r}_{23}|^3} + \dfrac{r_{24x}}{|\vec{r}_{24}|^3} \right) r_1 r_2 \mathrm{d}r_1 \mathrm{d}r_2 \mathrm{d}\alpha \mathrm{d}\beta \\ F_y = \dfrac{B_{r1}B_{r2}}{4\pi\mu_0} \cdot \int_{R_{1i}}^{R_{1o}}\int_{R_{2i}}^{R_{2o}}\int_0^{2\pi}\int_0^{2\pi} \left(+ \dfrac{r_{13y}}{|\vec{r}_{13}|^3} - \dfrac{r_{14y}}{|\vec{r}_{14}|^3} - \dfrac{r_{23y}}{|\vec{r}_{23}|^3} + \dfrac{r_{24y}}{|\vec{r}_{24}|^3} \right) r_1 r_2 \mathrm{d}r_1 \mathrm{d}r_2 \mathrm{d}\alpha \mathrm{d}\beta \\ F_z = \dfrac{B_{r1}B_{r2}}{4\pi\mu_0} \cdot \int_{R_{1i}}^{R_{1o}}\int_{R_{2i}}^{R_{2o}}\int_0^{2\pi}\int_0^{2\pi} \left(+ \dfrac{r_{13z}}{|\vec{r}_{13}|^3} - \dfrac{r_{14z}}{|\vec{r}_{14}|^3} - \dfrac{r_{23z}}{|\vec{r}_{23}|^3} + \dfrac{r_{24z}}{|\vec{r}_{24}|^3} \right) r_1 r_2 \mathrm{d}r_1 \mathrm{d}r_2 \mathrm{d}\alpha \mathrm{d}\beta \end{cases}, \quad (4)$$

where (see Fig. 1)

$$\vec{r}_{13} = \vec{y}_0 + \vec{z}_0 + \vec{x}_0 + \vec{l}_2 + \vec{r}_2 - (\vec{l}_1 + \vec{r}_1).$$

Therefore, the projection form and mode of vector $\vec{r}_{13}$ can be expressed as

$$\begin{cases} r_{13x} = x_0 - r_2 \sin\beta - l_1 \\ r_{13y} = y_0 + l_2 \sin\gamma + r_2 \cos\beta \cos\gamma - r_1 \cos\alpha \\ r_{13z} = z_0 + l_2 \cos\gamma - r_2 \cos\beta \sin\gamma - r_1 \sin\alpha \\ |\vec{r}_{13}| = \sqrt{r_{13x}^2 + r_{13y}^2 + r_{13z}^2} \end{cases}. \quad (5)$$

Similarly, the projection forms and modes of vectors $\vec{r}_{14}$, $\vec{r}_{23}$, and $\vec{r}_{24}$ can be expressed as

$$\begin{cases} r_{14x} = r_{13x} \\ r_{14y} = r_{13y} - 2l_2 \sin\gamma = y_0 - l_2 \sin\gamma + r_2 \cos\beta \cos\gamma - r_1 \cos\alpha \\ r_{14z} = r_{13z} - 2l_2 \cos\gamma = z_0 - l_2 \cos\gamma - r_2 \cos\beta \sin\gamma - r_1 \sin\alpha \\ |\vec{r}_{14}| = \sqrt{r_{14x}^2 + r_{14y}^2 + r_{14z}^2} \end{cases}, \quad (6)$$

$$\begin{cases} r_{23x} = r_{13x} + 2l_1 = x_0 - r_2 \sin\beta + l_1 \\ r_{23y} = r_{13y} \\ r_{23z} = r_{13z} \\ |\vec{r}_{23}| = \sqrt{r_{23x}^2 + r_{23y}^2 + r_{23z}^2} \end{cases}, \quad (7)$$

and

$$\begin{cases} r_{24x} = r_{23x} \\ r_{24y} = r_{23y} - 2l_2 \sin\gamma = y_0 - l_2 \sin\gamma + r_2 \cos\beta \cos\gamma - r_1 \cos\alpha \\ r_{24z} = r_{14z} \\ |\vec{r}_{24}| = \sqrt{r_{24x}^2 + r_{24y}^2 + r_{24z}^2} \end{cases}. \quad (8)$$

Substituting Eqs. (5)-(8) into Eq. (4), allows the components of the total interaction force to be calculated (the detailed final equations are not shown here for space considerations).

2.2. Torques between two perpendicular magnetic tubes

Torques between $\mathrm{MT_I}$ and $\mathrm{MT_{II}}$ are relative to the center of the torque. We discuss the particular case of torque of $\mathrm{d}\vec{F}_{13}$ around *O*, expressed by $\mathrm{d}\vec{T}_{13}$. Force $\mathrm{d}\vec{F}_{13}$ acts on point *P*, and the vector of $\mathrm{d}\vec{F}_{13}$ to *O* is $\vec{r}_{OP}$. From Fig. 1, the projection form of $\vec{r}_{OP}$ can be expressed as

$$\begin{cases} r_{OPx} = l_1 \\ r_{OPy} = r_1 \cos\alpha \\ r_{OPz} = r_1 \sin\alpha \end{cases}. \quad (9)$$

Hence, the torque of $\mathrm{d}\vec{F}_{13}$ around *O* can be expressed as

$$\mathrm{d}\vec{T}_{13} = \vec{r}_{OP} \times \mathrm{d}\vec{F}_{13} = \begin{vmatrix} \vec{i} & \vec{j} & \vec{k} \\ r_{OPx} & r_{OPy} & r_{OPz} \\ \mathrm{d}F_{13x} & \mathrm{d}F_{13y} & \mathrm{d}F_{13z} \end{vmatrix} = \begin{matrix} (r_1 \cos\alpha \mathrm{d}F_{13z} - r_1 \sin\alpha \mathrm{d}F_{13y})\vec{i} \\ +(r_1 \sin\alpha \mathrm{d}F_{13x} - l_1 \mathrm{d}F_{13z})\vec{j} \\ +(l_1 \mathrm{d}F_{13y} - r_1 \cos\alpha \mathrm{d}F_{13x})\vec{k} \end{matrix}, \quad (10)$$

where $\vec{i}$, $\vec{j}$, $\vec{k}$ are unit vectors of axes *Ox*, *Oy*, and *Oz*, respectively. Thus, Eq. (10) can be expressed as the projection form of $\mathrm{d}\vec{T}_{13}$,

$$\begin{cases} \mathrm{d}T_{13x} = r_1 \cos\alpha \mathrm{d}F_{13z} - r_1 \sin\alpha \mathrm{d}F_{13y} \\ \mathrm{d}T_{13y} = r_1 \sin\alpha \mathrm{d}F_{13x} - l_1 \mathrm{d}F_{13z} \\ \mathrm{d}T_{13z} = l_1 \mathrm{d}F_{13y} - r_1 \cos\alpha \mathrm{d}F_{13x} \end{cases}, \quad (11)$$

where $\mathrm{d}T_{13x}$, $\mathrm{d}T_{13y}$, and $\mathrm{d}T_{13z}$ are the projections of $\mathrm{d}\vec{T}_{13}$ to the *Ox*, *Oy*, and *Oz* axes, respectively.

Similarly, the projection forms of $\mathrm{d}\vec{T}_{23}$, $\mathrm{d}\vec{T}_{14}$, and $\mathrm{d}\vec{T}_{24}$, can be expressed as, respectively,

$$\begin{cases} \mathrm{d}T_{23x} = r_1 \cos\alpha \mathrm{d}F_{23z} - r_1 \sin\alpha \mathrm{d}F_{23y} \\ \mathrm{d}T_{23y} = r_1 \sin\alpha \mathrm{d}F_{23x} + l_1 \mathrm{d}F_{23z} \\ \mathrm{d}T_{23z} = -l_1 \mathrm{d}F_{23y} - r_1 \cos\alpha \mathrm{d}F_{23x} \end{cases}, \quad (12)$$

$$\begin{cases} \mathrm{d}T_{14x} = r_1 \cos\alpha \mathrm{d}F_{14z} - r_1 \sin\alpha \mathrm{d}F_{14y} \\ \mathrm{d}T_{14y} = r_1 \sin\alpha \mathrm{d}F_{14x} - l_1 \mathrm{d}F_{14z} \\ \mathrm{d}T_{14z} = l_1 \mathrm{d}F_{14y} - r_1 \cos\alpha \mathrm{d}F_{14x} \end{cases}, \quad (13)$$

and

$$\begin{cases} \mathrm{d}T_{24x} = r_1 \cos\alpha \mathrm{d}F_{24z} - r_1 \sin\alpha \mathrm{d}F_{24y} \\ \mathrm{d}T_{24y} = r_1 \sin\alpha \mathrm{d}F_{24x} + l_1 \mathrm{d}F_{24z} \\ \mathrm{d}T_{24z} = -l_1 \mathrm{d}F_{24y} - r_1 \cos\alpha \mathrm{d}F_{24x} \end{cases}. \quad (14)$$

Thus,

$$\begin{cases} \mathrm{d}T_x = \mathrm{d}T_{13x} + \mathrm{d}T_{14x} + \mathrm{d}T_{23x} + \mathrm{d}T_{24x} \\ \mathrm{d}T_y = \mathrm{d}T_{13y} + \mathrm{d}T_{14y} + \mathrm{d}T_{23y} + \mathrm{d}T_{24y} \\ \mathrm{d}T_z = \mathrm{d}T_{13z} + \mathrm{d}T_{14z} + \mathrm{d}T_{23z} + \mathrm{d}T_{24z} \end{cases}, \quad (15)$$

and, combining Eqs. (2) and (11)-(15),

$$\begin{cases} T_x = \dfrac{B_{r1}B_{r2}}{4\pi\mu_0}\displaystyle\int_{R_{1i}}^{R_{1o}}\int_{R_{2i}}^{R_{2o}}\int_0^{2\pi}\int_0^{2\pi}\left(A_1\cos\alpha + A_2\sin\alpha\right)r_1^2 r_2\,\mathrm{d}\alpha\,\mathrm{d}\beta\,\mathrm{d}r_1\,\mathrm{d}r_2 \\ T_y = \dfrac{B_{r1}B_{r2}}{4\pi\mu_0}\displaystyle\int_{R_{1i}}^{R_{1o}}\int_{R_{2i}}^{R_{2o}}\int_0^{2\pi}\int_0^{2\pi}\left(A_3 r_1\sin\alpha + A_4 l_1\right)r_1 r_2\,\mathrm{d}\alpha\,\mathrm{d}\beta\,\mathrm{d}r_1\,\mathrm{d}r_2 \\ T_z = \dfrac{B_{r1}B_{r2}}{4\pi\mu_0}\displaystyle\int_{R_{1i}}^{R_{1o}}\int_{R_{2i}}^{R_{2o}}\int_0^{2\pi}\int_0^{2\pi}\left(A_5 l_1 + A_6 r_1\cos\alpha\right)r_1 r_2\,\mathrm{d}\alpha\,\mathrm{d}\beta\,\mathrm{d}r_1\,\mathrm{d}r_2 \end{cases}, \quad (16)$$

where

$$A_1 = +\frac{r_{13z}}{|\vec{r}_{13}|^3} - \frac{r_{23z}}{|\vec{r}_{23}|^3} - \frac{r_{14z}}{|\vec{r}_{14}|^3} + \frac{r_{24z}}{|\vec{r}_{24}|^3},\quad A_2 = -\frac{r_{13y}}{|\vec{r}_{13}|^3} + \frac{r_{23y}}{|\vec{r}_{23}|^3} + \frac{r_{14y}}{|\vec{r}_{14}|^3} - \frac{r_{24y}}{|\vec{r}_{24}|^3},$$

$$A_3 = +\frac{r_{13x}}{|\vec{r}_{13}|^3} - \frac{r_{23x}}{|\vec{r}_{23}|^3} - \frac{r_{14x}}{|\vec{r}_{14}|^3} + \frac{r_{24x}}{|\vec{r}_{24}|^3},\quad A_4 = -\frac{r_{13z}}{|\vec{r}_{13}|^3} - \frac{r_{23z}}{|\vec{r}_{23}|^3} + \frac{r_{14z}}{|\vec{r}_{14}|^3} + \frac{r_{24z}}{|\vec{r}_{24}|^3},$$

$$A_5 = +\frac{r_{13y}}{|\vec{r}_{13}|^3} + \frac{r_{23y}}{|\vec{r}_{23}|^3} - \frac{r_{14y}}{|\vec{r}_{14}|^3} - \frac{r_{24y}}{|\vec{r}_{24}|^3},\ \text{and}\ A_6 = -\frac{r_{13x}}{|\vec{r}_{13}|^3} + \frac{r_{23x}}{|\vec{r}_{23}|^3} + \frac{r_{14x}}{|\vec{r}_{14}|^3} - \frac{r_{24x}}{|\vec{r}_{24}|^3}.$$

Substituting Eqs. (5)-(8) into Eq. (16), the components of the total interaction torque can be calculated (the detailed final equations are not shown here for space considerations).

3. Numerical Analysis of Interaction Forces and Torques

Interaction forces and torques expressions are somewhat complicated, which makes it difficult to derive the analytical forms. Fortunately, there are many convenient software packages and good performance personal computers, using the Gauss-Legendre integration method, the numerical solution can be performed conveniently and rapidly.

Table 1 shows the parameters [30] and geometry dimensions of the NdFeB permanent magnets. According to the relative positions and inclined angle of MT_{II}, changes for interaction forces and torques with three coordinate axes and the inclined angle are calculated.

Table 1. NdFeB material parameters and magnetic tube dimensions.

Material parameters	Magnetic tube dimensions
Remanence, $B_r = 1.298$ T	MT_I Length, $2l_1 = 0.020$ m Inner radius, $R_{1i} = 0.020$ m Outer radius, $R_{1o} = 0.040$ m
Coercive force, $H_c = 900$ kA·m	
Energy product, $(BH)_{max} = 305$ kJ·m^{-3}	MT_{II} Length, $2l_2 = 0.020$ m Inner radius, $R_{2i} = 0.020$ m Outer radius, $R_{2o} = 0.040$ m

3.1. Influence of displacement on interaction forces and torques

Figure 2 shows the relationship between interaction forces, torques, and tube axes when the center of MT_{II}, O_2, is on the axes of coordinate $Oxyz$.

Figures 2(a) and 2(b) show the components of interaction forces and torques, respectively, when $y_0 = z_0 = 0$, $\gamma = 0$, and O_2 is moving along the Ox axis. Forces F_x and F_y, and torques T_x and T_z are constantly zero with changing x_0. Force F_z and torque T_y have their extreme values (40N and –2.9 N·m, respectively) when x_0 = 50 mm, which means that the extreme values appear when the tubes are contacting.

Figures 2(c) and 2(d) show the components of interaction forces and torques, respectively, when $x_0 = z_0 = 0$, $\gamma = 0$, and O_2 is moving along the Oy axis. Forces F_x, F_y, and F_z, and torques T_x and T_z, are constantly zero with changing y_0. Torque T_y has extreme value (2.6 N·m) when the tubes are contacting (y_0 = 80 mm).

Figures 2(e) and 2(f) show the components of interaction forces and torques, respectively, when $x_0 = y_0 = 0$, $\gamma = 0$, and O_2 is moving along the Oz axis. Forces F_y and F_z, and torques T_x and T_z are constantly zero with changing z_0. Force F_x is as the same as F_z in Fig. 2(a), and T_y

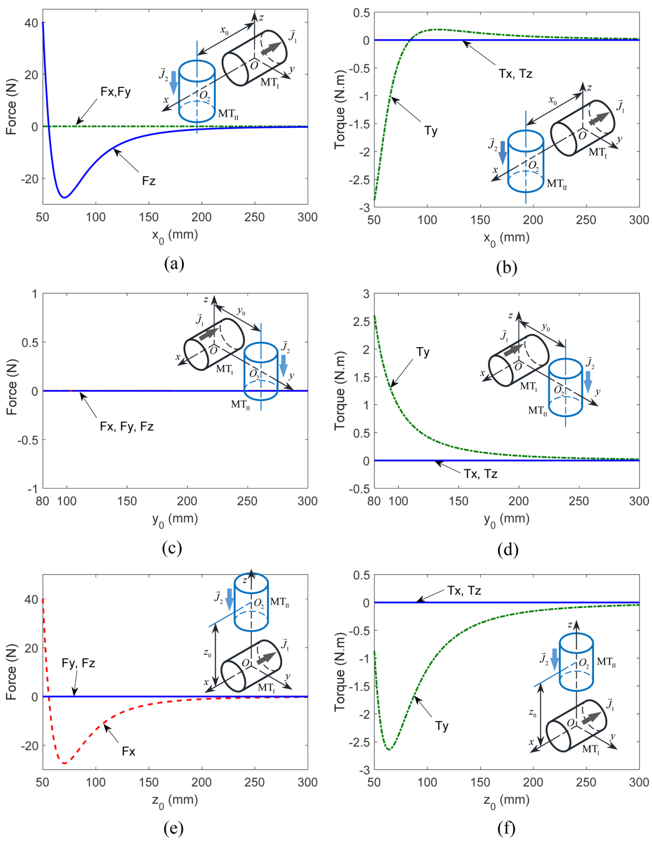

Fig. 2. (Color online) Relationships between interaction forces, torques, and tube axes.

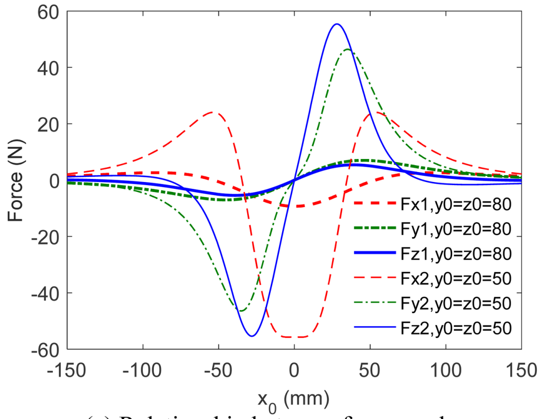

(a) Relationship between forces and x_0

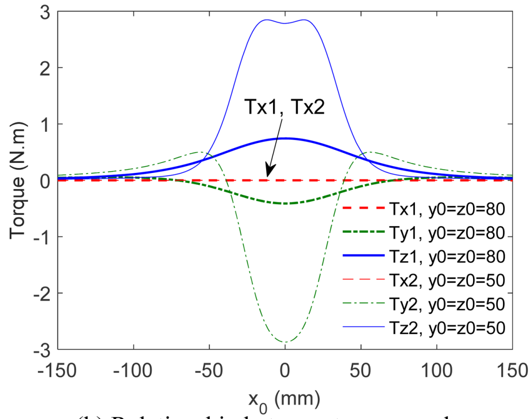

(b) Relationship between torques and x_0

Fig. 3. (Color online) Relationships of interaction forces and torques with x_0 (g = 0, y_0 = z_0).

reaches extreme value (2.6 N·m) when z_0 = 64 mm.

Figures 3(a) and 3(b) show the components of interaction forces and torques, respectively, for varying x_0 when O_2 is not on $Oxyz$, such as γ = 0, y_0 = z_0 = 50 or 80 mm. Force and torque extreme values increase with decreasing z_0, because the force between two magnetic charges increases with decreasing distance between the charges.

3.2. Influence of the inclined angle on interaction forces and torques

Figure 4 shows the influence of γ on the interaction forces and torques. Figures 4(a) and 4(b) show the relationships of interaction forces and torques, respectively, with γ when y_0 = z_0 = 0, and x_0 = 100 mm. F_x and T_x, are constantly zero, while F_y, F_z, T_y, and T_z, follow a sinusoidal pattern, with initial phase difference π/2.

Figures 4(c) and 4(d) show the relationships of interaction forces and torques, respectively, with γ when x_0 = z_0 = 0, y_0 = 100 mm. F_x, T_y, and T_z, changing periodically with 2π. The other forces and torques are constantly zero.

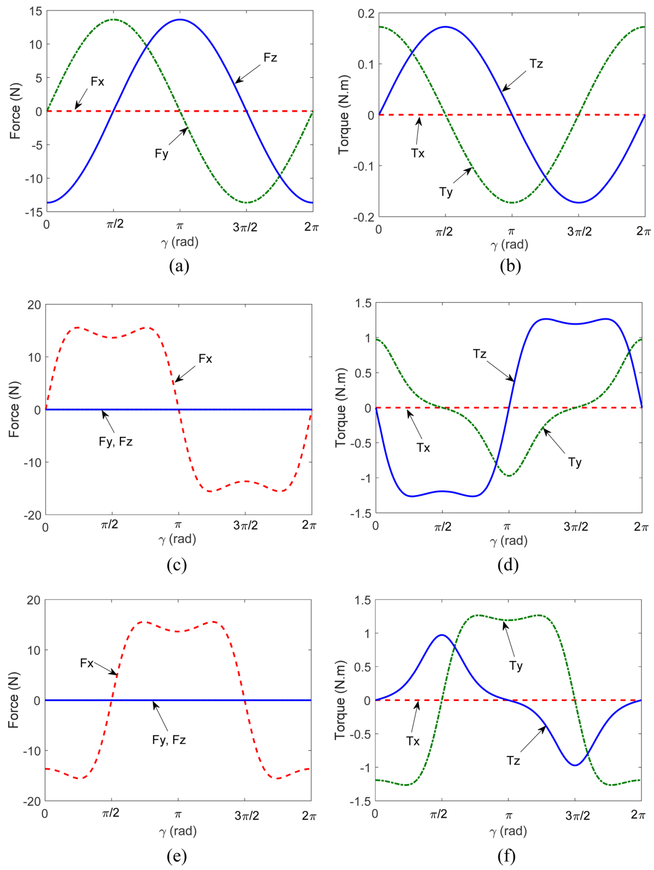

Fig. 4. (Color online) Relationships of interaction forces and torques with the inclined angle, γ.

Figures 4(e) and 4(f) show the relationships of interaction forces and torques, respectively, with γ when x_0 = y_0 = 0, z_0 = 100 mm. The forces are similar to Fig. 4(c), with F_x lagging a quarter of a cycle; T_x is constantly zero; T_z is similar to T_y in Fig. 4(c), but ahead quarter of a cycle; and T_y, is similar to T_z in Fig. 4(c), but lags a quarter of a cycle.

4. Conclusions

The following conclusions can be derived from this study.

(a) A mathematical model of forces and torques between two perpendicular magnetic tubes was successfully derived using the theory of magnetic charges and magnetic Coulomb's law.

(b) Forces and torques between two perpendicular magnetic tubes can be obtained numerically from the model. When the inclined angle, γ = 0, and the tubes are contacting, it means x_0 = 50 mm, y_0 = z_0 = 0, force F_z reaches its extreme value of 40N and torque T_y reaches its extreme value of –2.9N·m.

(c) The model can also be used to calculate the forces and torques between two perpendicular magnetic cylinders or tubes or a cylinder and a tube.

(d) This work provides theoretical guidance for engineering applications of perpendicular magnetic tubes or cylinders.

Acknowledgments

This work was supported financially by the Doctoral Scientific Research Foundation of Yanbian University (No. 602016002).

References

[1] M. Hutterer, G. Kalteis, and M. Schrödl, Mech. Syst. Signal Pr. **94**, 267 (2017).
[2] A. E. Jahromi and F. K. Miller, Cryogenics **82**, 68 (2017).
[3] C. W. Kim and J. Y. Choi, J. Magnetics **21**, 110 (2016).
[4] K. Shin, J. Vibroeng. **16**, 1745 (2014).
[5] G. E. Mann, A. Canter, S. Nair, D. LaMonica, M. Kahana, J. Yoo, and E. Delphin, ACTA Paediatr. **106**, 1001 (2017).
[6] S. Yuan, Y. Huang, J. Zhou, Q. Xu, C. Song, and G. Yuan, IEEE T. Power Electr. **32**, 5365 (2017).
[7] J. F. Charpentier and G. Lemarquand, IEEE Trans. Magn. **35**, 4206 (1999).
[8] Z. J. Liu, J. L. Li, and M. A. Jabbar, J. Appl. Phys. **99**, 08R321 (2006).
[9] J. L. G. Janssen, J. J. H. Paulides, J. C. Compter, and E. Lomonova, IEEE Trans. Magn. **46**, 1748 (2010).
[10] J. J. Sun, Y. Ren, and J. C. Fang, J. Magn. Magn. Mater. **323**, 2103 (2011).
[11] P. Kim and J. Seok, Mech. Mach. **94**, 41 (2015).
[12] J. Zhao, R. Gao, G. Chen, S. Liu, Q. Cao, and T. Qiu, Mech. Mach. **83**, 56 (2015).
[13] J. Sun, C. Wang, and Y. Le, IEEE-ASME T. Mech. **21**, 2881 (2016).
[14] G. Akoun and J. P. Yonnet, IEEE Trans. Magn. **20**, 1962 (1984).
[15] H. Allag and J. P. Yonnet, IEEE Trans. Magn. **45**, 3969 (2009).
[16] H. Allag, J. P. Yonnet, M. Fassenet, and M. E. Latreche, Sensor Lett. **7**, 486 (2009).
[17] J. L. G. Janssen, J. J. H. Paulides, E. Lomonova, F. Bölöni, A. Tounz, and F. Periou, Sensor Lett. **7**, 442 (2009).
[18] H. Allag, J. P. Yonnet, and M. E. Latreche, J. Appl. Phys. **107**, 07E701 (2011).
[19] P. Eliès and G. Lemarquand, IEEE Trans. Magn. **34**, 2267 (1998).
[20] D. Vokoun, M. Beleggia, L. Heller, and P. Šittner, J. Magn. Magn. Mater. **321**, 3758 (2009).
[21] J. S. Agashe and D. P. Arnold, J. Phys. D: Appl. Phys. **41**, 105001 (2008).
[22] M. Greconici, “Analytical-Numerical Approach for Levitation Force Calculation of a Cylindrical Bearing with Permanent Magnets Used in an Electric Meter”, IEEE OPTIM 12th International conference (2010).
[23] M. I. González, Eur. J. Phys. **38**, 025202 (2017).
[24] D. Vokoun, G. Tomassetti, M. Beleggia, and I. Stachiv, J. Magn. Magn. Mater. **323**, 55 (2011).
[25] D. Vokoun and M. Beleggia, J. Magn. Magn. Mater. **350**, 174 (2014).
[26] O. J. Suarez, P. Vargas, and E. E. Vogel, J. Magn. Magn. Mater. **321**, 3658 (2009).
[27] D. Vokoun, M. Beleggia, and L. Heller, J. Magn. Magn. Mater. **324**, 1715 (2012).
[28] Q. C. Tan, W. Li, and B. Liu, Tribol. Int. **35**, 443 (2002).
[29] Q. C. Tan, Z. Q. Kou, W. Li, and Y. C. Pei, Int. J. Appl. Electrom. **20**, 71 (2004).
[30] Q. C. Tan, F. S. Zheng, and J. G. Li, J. Bionic. Eng. **5**, 143 (2008).
[31] Q. C. Tan, D. Xin, W. Li, and H. Meng, P. I. Mech. Eng. C-J Mec. **206**, 381 (1992).